Volume 9 | Number 46 | 14 December 2017 | Pages 18113–18562

Nanoscale

rsc.li/nanoscale

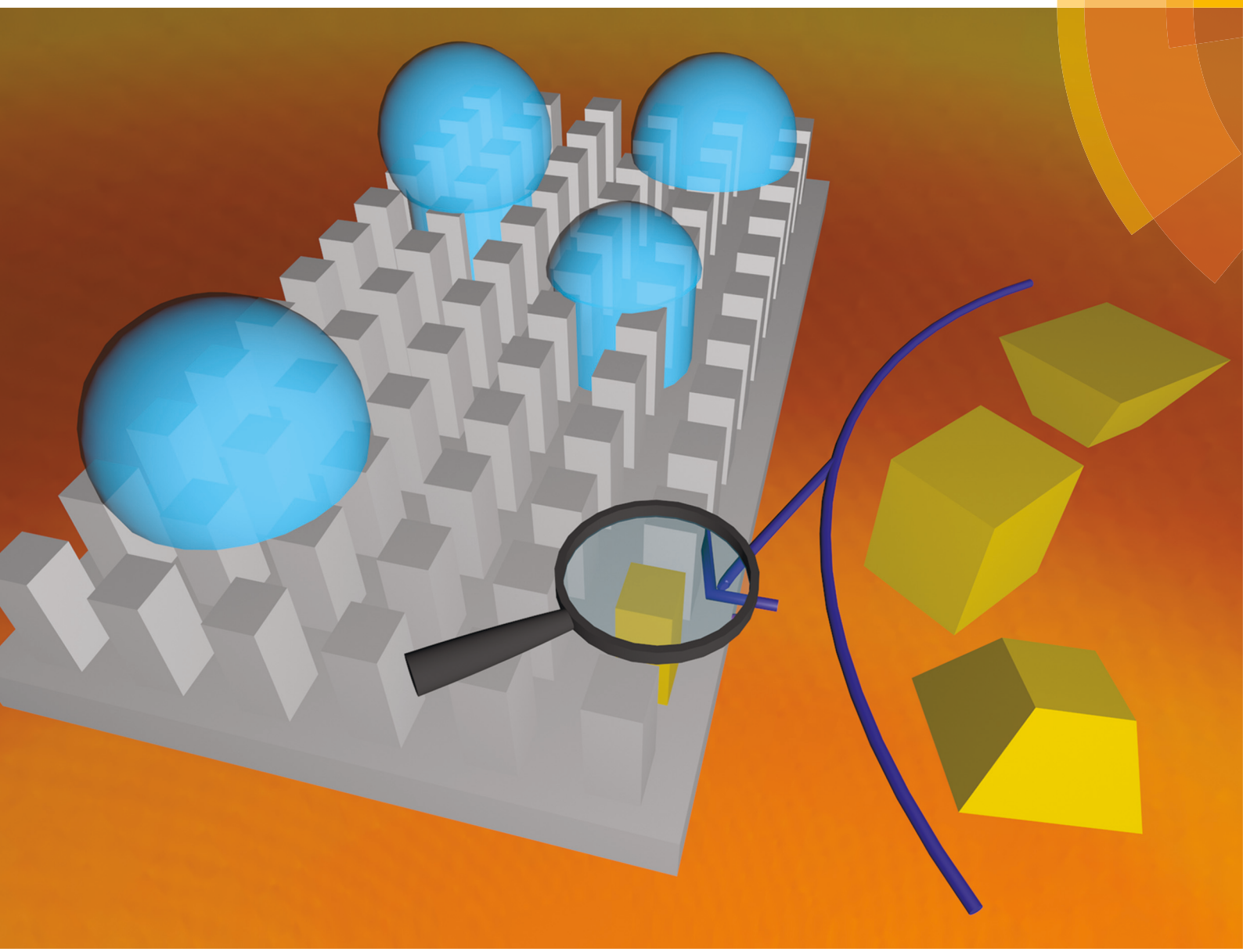

ISSN 2040-3372

ROYAL SOCIETY OF CHEMISTRY

PAPER

Joseph S. Francisco, Xiao Cheng Zeng *et al.*

Controlling states of water droplets on nanostructured surfaces by design

NCNST

Nanoscale

PAPER

Cite this: *Nanoscale*, 2017, **9**, 18240

Controlling states of water droplets on nanostructured surfaces by design†

Chongqin Zhu,‡[a,b] Yurui Gao,‡[c] Yingying Huang,[d] Hui Li,[b] Sheng Meng,[e] Joseph S. Francisco*[a] and Xiao Cheng Zeng*[a,b]

Received 15th September 2017,
Accepted 24th October 2017

DOI: 10.1039/c7nr06896d

rsc.li/nanoscale

Surfaces that exhibit both superhydrophobic and superoleophobic properties have recently been demonstrated. Specifically, remarkable designs based on overhanging/inverse-trapezoidal microstructures enable water droplets to contact these surfaces only at the tips of the micro-pillars, in a state known as the Cassie state. However, the Cassie state may transition into the undesirable Wenzel state under certain conditions. Herein, we show from large-scale molecular dynamics simulations that the transition between the Cassie and Wenzel states can be controlled *via* precisely designed trapezoidal nanostructures on a surface. Both the base angle of the trapezoids and the intrinsic contact angle of the surface can be exploited to control the transition. For a given base angle, three regimes can be achieved: the Wenzel regime, in which water droplets can exist only in the Wenzel state when the intrinsic contact angle is less than a certain critical value; the Cassie regime, in which water droplets can exist only in the Cassie state when the intrinsic contact angle is greater than another critical value; and the bistable Wenzel–Cassie regime, in which both the Wenzel and Cassie states can exist when the intrinsic contact angle is between the two critical values. A strong base-angle dependence of the first critical value is revealed, whereas the second critical value shows much less dependence on the base angle. The stability of the Cassie state for various base angles (and intrinsic contact angles) is quantitatively evaluated by computing the free-energy barrier for the Cassie-to-Wenzel state transition.

1. Introduction

The ability to control the wettability of a surface is crucial in a variety of applications,[1–5] including self-cleaning surfaces,[1] microfluidics,[2,3] heat transfer[4] and water/oil separation.[5] It is well known that the hydrophobicity of a surface depends on both the chemical composition[6–10] and physical topography[11,12] of the surface. Given the limitations of controlling the wetting properties of a flat surface *via* chemical modification,[6,7] physical modifications to create various micro- or nanostructured surfaces have been extensively explored.[13–29] In fact, nature provides the first examples of microstructured superhydrophobic surfaces, such as lotus leaves and water striders' non-wetting legs.[30–32]

The wettability of rough surfaces has been understood *via* the classical Cassie model[12] and the Wenzel model.[11] The Wenzel model assumes that the liquid droplet wets the entire rough substrate, whereas the Cassie model assumes that the droplet is in partial contact with the rough substrate (*i.e.*, the topmost part of the substrate). In contrast to the Wenzel model, the Cassie model allows for the possibility of $\theta_a > 90°$ when $\theta_{in} < 90°$, where θ_a and θ_{in} are the apparent and intrinsic contact angles of the corresponding rough and flat surfaces, respectively.[33] Thermodynamic conditions can be used to determine the wetting state of a droplet on a particular textured surface.[33–35] The threshold value of the equilibrium contact angle, θ_c, for the transition from the Wenzel to the Cassie state is given by[36]

$$\cos\theta_c = \frac{(\varphi_s - 1)}{(r - \varphi_s)} \quad (1)$$

where r (≥ 1) is the roughness factor, defined as the ratio of the specific area to the projected area, and φ_s is the ratio of the

[a]*Department of Chemistry, University of Nebraska—Lincoln, Lincoln, Nebraska 68588, USA. E-mail: jfrancisco3@unl.edu, xzeng1@unl.edu*
[b]*Beijing Advanced Innovation Center for Soft Matter Science and Engineering, Beijing University of Chemical Technology, Beijing 100029, China*
[c]*Department of Physics and Astronomy, California State University Northridge, Northridge, California 91330-8268, USA*
[d]*Key Laboratory of Materials Modification by Laser, Ion and Electron Beams (Dalian University of Technology), Ministry of Education, Dalian 116024, China*
[e]*Beijing National Laboratory for Condensed Matter Physics and Institute of Physics, Chinese Academy of Sciences, Collaborative Innovation Center of Quantum Matter, Beijing, 100190, China*

†Electronic supplementary information (ESI) available: Wettability of modelled surface, potential profile and "raining" simulations. See DOI: 10.1039/c7nr06896d

‡These authors contributed equally to this work.

area of the actual contact interface between the droplet and the substrate to the area of the projected interface underneath the droplet. If $\theta_{in} > \theta_c$, the droplet will be in the Cassie state, and if $\theta_{in} < \theta_c$, the droplet will be in the Wenzel state. As $r \geq 1 \geq \varphi_s$, the θ_c value for this transition is necessarily greater than 90°, which indicates that a surface cannot exist in the Cassie state for $\theta_{in} < 90°$. These arguments highlight the challenge of designing a superhydrophobic surface based on hydrophilic materials (defined as materials with $\theta_{in} < 90°$).

However, some recent studies have suggested the possibility of fabricating superhydrophobic surfaces from intrinsically hydrophilic materials.[13,14,21,25,29,37–40] Herminghaus found that the leaves of plants such as *Cotinus coggygria* and *Ginkgo biloba* show unexpectedly high non-wetting properties even for $\theta_{in} < 90°$.[39] Cheng *et al.* showed that the wax on lotus leaves has a θ_{in} value of ~74° rather than a value of $\theta_{in} > 90°$ as expected.[24] Recently, overhanging shelves on the tops of micropillars have been introduced to render even a surface with $\theta_{in} = 0°$ (ref. 13) superoleophobic. The superhydrophobic state of these textured surfaces is a metastable Cassie state rather than the equilibrium Wenzel state. Overhanging and trapezoidal microstructures have also been utilized in several studies to realize highly non-wetting surfaces.[13,14,41,42] In fact, overhanging and pillared structures can be regarded as special cases of trapezoidal structures with $\varphi = 0°$ and $\varphi = 90°$, respectively (here, φ is the base angle of the trapezoid).

Despite the reported fabrication of superhydrophobic surfaces from hydrophilic materials, the mechanisms of how the surface geometry and the surface's intrinsic hydrophobicity affect the Cassie-to-Wenzel transition, especially the stability of the Cassie state, have still been little studied. Herein, using classical molecular dynamics (MD) simulations, we investigated three conditions that can affect the transition between the Wenzel and Cassie states on a surface with trapezoidal nanostructures: (i) the base angle of the trapezoid structure, as measured from the top to the inclined side; (ii) the intrinsic contact angle of a droplet on the flat surface; and (iii) the impinging velocity of a water nanodroplet. For a given trapezoid base angle, the following three regimes exist: (i) the Wenzel regime, in which a water droplet can exist only in the Wenzel state and when the intrinsic contact angle is smaller than a certain critical value; (ii) the Cassie regime, in which a water droplet can exist only in the Cassie state and when the intrinsic contact angle is larger than another critical value; and (iii) the Wenzel–Cassie regime, in which bistable Wenzel and Cassie states can arise and when the intrinsic contact angle is between the two critical values. For the bistable Wenzel–Cassie regime, the free-energy barrier for the Cassie-to-Wenzel state transition was computed to examine the influence of the trapezoid base angle on the relative stability of the Cassie state on surfaces with various wettabilities.

2. Methods

2.1 Simulation set-up

The surfaces considered in this study consisted of atoms arranged in a cubic lattice with a lattice spacing of 4 Å. The atoms of the solid surface remained fixed throughout the simulations. The basal surface, which was situated at the bottom of the simulation box, consisted of five layers of atoms and was 20 Å thick. Trapezoidal convexities with an upper width of W = 24.0 Å and a height of H = 14.0 Å were used to create the surface texture. The convexities were arranged on a square lattice with a spacing of S = 40.0 Å. The base angle of the trapezoids was varied from 45° to 120°. A pre-equilibrated water cube consisting of 24 256 molecules was used in our simulations. The lateral size of the solid surface was 200 × 200 Å. The length of the simulation cell was 270 Å, three times the side length of the water cube.

2.2 Simulation details

Owing to the large size of the system, the coarse-grained mW water model,[43] in which each water molecule is treated as a single particle interacting through anisotropic short-ranged potentials (the Stillinger–Weber potential), was chosen. Although explicit hydrogen atoms and electrostatic terms are not included, the mW model can correctly describe the thermodynamic properties and phase behaviour of water both in bulk and in confinement.[44–48] The surface atoms interacted with each water molecule through the 12–6 Lennard-Jones (LJ) potential with σ_{SW} = 3.2 Å, and ε_{SW} was varied from 0.289 kJ mol^{-1} to 1.544 kJ mol^{-1} on modelled surfaces ranging from hydrophobic to hydrophilic. Periodic boundary conditions were applied in three dimensions, and the equations of motion were integrated using the velocity Verlet algorithm with a time step of 10 fs. Simulations were performed using an NVT ensemble, in which the temperature was controlled at 300 K using the Nosé–Hoover thermostat and the relaxation time was 0.1 ps. All simulations were performed using the Large-scale Atomic/Molecular Massively Parallel Simulator (LAMMPS) software.[49]

2. Results and discussion

To measure the wettability of each modelled surface, we first computed the intrinsic contact angle (θ_{in}) of a water droplet on the corresponding flat surface. To this end, a series of classical MD simulations were performed (see ESI Fig. S1 and S2†). The intrinsic contact angle is defined as the angle between a line tangent to the droplet at the three-phase contact point and a line parallel to the flat surface (see ref. 50 for the detailed computational method). In our simulations, the interaction parameter between a water molecule and an atom of the solid surface (ε) was tuned from 0.289 kJ mol^{-1} to 1.544 kJ mol^{-1}, and the corresponding computed θ_{in} values ranged from 58° to 149° (ESI Fig. S3†). According to a previous study, $\cos\theta_{in}$ exhibits a linear dependence on ε.[51] The red dashed line in ESI Fig. S3† represents a linear fit to all data points (with $\theta_{in} > 0$) using the least-squares algorithm. The fitted straight line is described by

$$\cos\theta_{in} = 1.133\varepsilon - 1.263. \quad (2)$$

Next, a second series of independent MD simulations were performed, in which the surface was covered with a periodic array of trapezoids, to investigate the effects of the trapezoid base angle (φ) and the intrinsic contact angle (θ_{in}) of the surface on the wetting state of a water nanodroplet. Initially, a cuboid box of 24 256 water molecules with dimensions of 90 × 90 × 90 Å was placed on top of the trapezoids (Fig. 1). The trapezoid base angle (φ) was varied from 45° to 120.0°. Here, four different systems were studied, each equilibrated for 2 ns. Snapshots of the equilibrated droplets at t = 2.0 ns for φ = 45° on surfaces with different intrinsic contact angles (θ_{in}) are shown in Fig. 2ai–aiv.

Our results show that the final state of the droplet is very sensitive to θ_{in} (Fig. 2a). For all cases with θ_{in} > 53.8°, the droplet favours the Cassie state (Fig. 2ai and 2aii). For all cases with θ_{in} < 50.7°, the droplet adopts the Wenzel state (Fig. 2aiii and 2aiv). Thus, we estimate the critical intrinsic contact angle (θ_{in}^{cw}) to be approximately 52.8° ± 1.0°, below which only the Wenzel state exists. For φ = 60°, the value of θ_{in}^{cw} is estimated to be 78.9° ± 0.6°; for φ = 90°, θ_{in}^{cw} = 106.1° ± 1.3°; and for φ = 120°, θ_{in}^{cw} = 126.0° ± 1.5° (Fig. 2av–axvi). In addition to recording snapshots of the equilibrated droplet, we also monitored how the potential energy of the water molecules changed with θ_{in} (ESI Fig. S4†) to characterize the state of the droplet. The θ_{in}^{cw} values obtained by analysing the variation in the potential energy with θ_{in} agree with those obtained based on the snapshots. Clearly, the critical intrinsic contact angle for the transition from the Cassie to the Wenzel state (θ_{in}^{cw}) shows a large variation with respect to the trapezoid base angle (φ), with θ_{in}^{cw} increasing as φ increases (solid black circles in Fig. 3). By fitting an exponential curve to the θ_{in}^{cw} *versus* φ data, we deduced the following relation: $\cos\theta_{in}^{cw} \approx -0.68 + 0.37\exp(1.77\cos\varphi)$ (solid black line in Fig. 3).

In addition to the transition from the Cassie to the Wenzel state, the reverse transition from the Wenzel to the Cassie state was also observed in our MD simulations of water nanodroplets on trapezoid-structured surfaces with the initial droplet location at the bottom of the grooves (ESI Fig. S5†). Snapshots of the equilibrated droplets for φ = 45° are shown in Fig. 2bi–

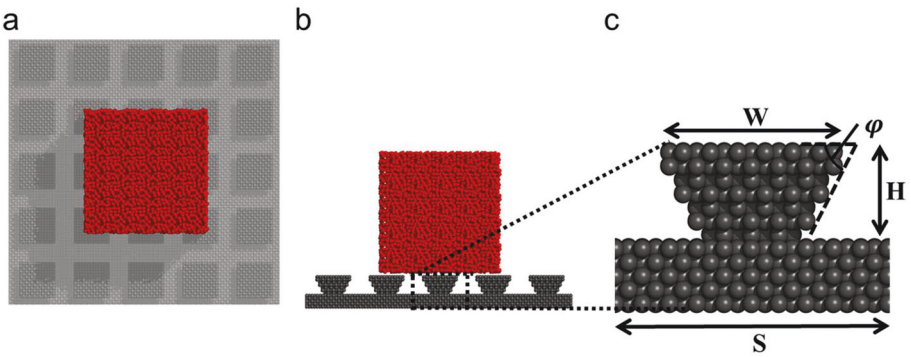

Fig. 1 Top and side views of the initial water droplet (red cube) in the Cassie state on a surface with trapezoidal nanostructures (a, b). A zoomed-in view of a surface structure is shown in (c). The width of the upper part of the trapezoid is W = 24.0 Å, its height is H = 14.0 Å, and the length of each trapezoid unit is S = 40.0 Å. The trapezoid base angle, φ, was varied from 45° to 120°.

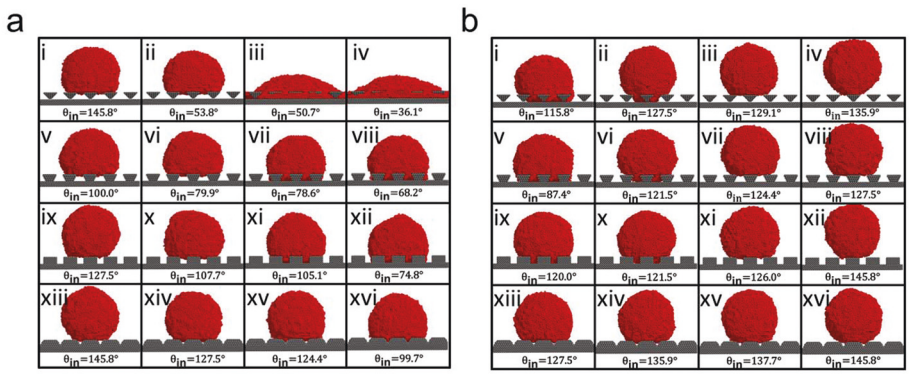

Fig. 2 Snapshots of systems at t = 2.0 ns from MD simulations with (a) initial configurations with the water droplet (red cube) in the Cassie state and (b) initial configurations with the water droplet in the Wenzel state. The intrinsic contact angle of the surface, θ_{in}, is shown below each snapshot. Four trapezoid base angles, *i.e.*, φ = 45° (ai–aiv, bi–biv), φ = 60° (av–aviii, bv–bviii), φ = 90° (aix–axii, bix–bxii) and φ = 120° (axiii–axvi, bxiii–bxvi), were selected for the MD simulations.

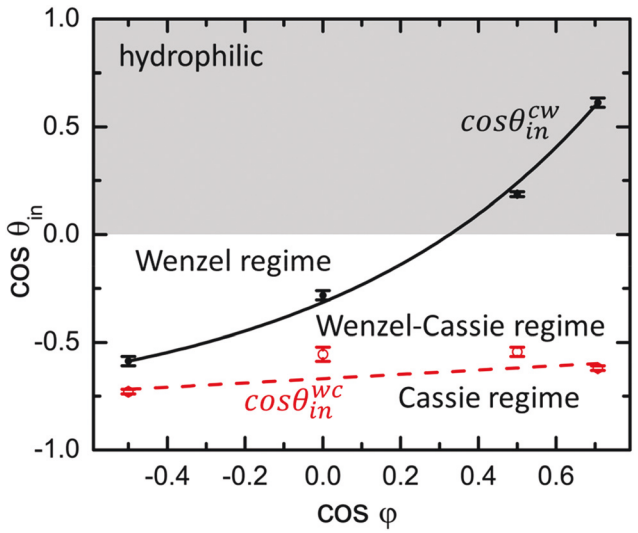

Fig. 3 Variation of the cosines of the two critical intrinsic contact angles, θ_{in}^{cw} (solid black circles) and θ_{in}^{wc} (open red circles), with the cosine of the trapezoid base angle based on the MD simulations. The solid black and dashed red curves represent exponential fits to $\cos\theta_{in}^{cw}$ and $\cos\theta_{in}^{wc}$, respectively. When $\theta_{in} < \theta_{in}^{cw}$, the Wenzel state is the only stable state for the droplet (above the solid black line), and when $\theta_{in} > \theta_{in}^{wc}$, the Cassie state is the only stable state (below the dashed red line).

biv. The final state of the droplet is the Cassie state when $\theta_{in} > 129.1°$ (Fig. 2biii and 2biv), whereas the droplet favours the Wenzel state when $\theta_{in} < 127.5°$ (Fig. 2bi and 2bii), indicating that the Cassie state is the only stable state when $\theta_{in} > 128.3° \pm 0.8°$. Additional simulations were performed to determine the critical intrinsic contact angles (θ_{in}^{wc}) for other values of φ (ESI Fig. S6, S7† and Fig. 2bv–bxvi). The calculated θ_{in}^{wc} values for $\varphi = 60°$, $\varphi = 90°$ and $\varphi = 120°$ are $122.9° \pm 1.5°$, $123.8° \pm 2.3°$ and $136.8° \pm 0.9°$, respectively. In contrast to the transition from the Cassie to the Wenzel state, the critical intrinsic contact angle for the Wenzel-to-Cassie state transition (θ_{in}^{wc}) shows only a slight variation with the trapezoid base angle (φ) (see the open red circles in Fig. 3).

Our MD simulations show that for a given φ, there exist two critical intrinsic contact angles, *i.e.*, θ_{in}^{cw} and θ_{in}^{wc}. When $\theta_{in} < \theta_{in}^{cw}$, the Wenzel state is the only stable state for the droplet (phase region above the solid black line in Fig. 3), and when $\theta_{in} > \theta_{in}^{wc}$, the Cassie state is the only stable state (phase region below the dashed red line in Fig. 3). Hence, both the Wenzel and Cassie states can exist for the water droplet when $\theta_{in}^{cw} < \theta_{in} < \theta_{in}^{wc}$ (region between the solid black and dashed red lines in Fig. 3).

To gain more insight into the relative stability of the Cassie state, it is important to obtain quantitative values of the free-energy barrier for the transition from the Cassie to the Wenzel state at a given base angle (φ) and different intrinsic contact angles (θ_{in}). Towards this end, "raining" simulations mimicking macroscopic raining experiments were performed.[16] Prior to the raining simulations, MD simulations of a water nanodroplet (24 256 water molecules) at a temperature of $T = 300$ K were performed for 1 ns to obtain the equilibrium configurations and initial velocities. Then, a nanodroplet was placed 60 Å above the simulated surface with a downward velocity v_d imposed instantaneously on all water molecules (ESI Fig. S8a†). The raining experiments were performed in an ensemble of constant volume and constant total energy (an NVE ensemble). It is worth mentioning that a previous study showed that the free-energy barrier separating the Cassie and Wenzel state is not sensitive to the size of water nanodroplet when water nanodroplet is large enough (greater than about 1700 water molecules),[16] suggesting that conclusions drawn from nanoscale droplet simulation for the relative stability of Cassie/Wenzel states could be extended to microscale droplets.

When $\theta_{in}^{cw} < \theta_{in} < \theta_{in}^{wc}$, both the Cassie and Wenzel states can be observed if the downward velocity v_d is appropriate (ESI Fig. S8, ESI Movies S1 and S2†). In the raining simulations, 120 completely independent MD simulations were performed for each given v_d, and the numbers of events in which the droplet was in the Cassie and Wenzel states were recorded (Table S1†). Six or seven downward velocities were selected for each given (φ, θ_{in}). For each given v_d, the probability P_w for the droplet to be in the Wenzel state was computed, as shown in Tables S1 and S2.† According to a previous study,[16] P_w can be fitted to an exponential equation as follows:

$$P_w = P_0 \exp\left(-\frac{\Delta G_{cw}}{e_k}\right), \quad (3)$$

where P_0, ΔG_{cw} and e_k are the pre-exponential factor, the free-energy barrier for the Cassie-to-Wenzel state transition and the kinetic energy (per molecule) of the centre of mass of the droplet, respectively. The variation of $\ln P_w$ with $1/e_k$ is shown in Fig. 4a for all θ_{in} values considered for $\varphi = 45°$. A linear fit to $\ln P_w$ *versus* $1/e_k$ indicates a free-energy barrier of $\Delta G_{cw} = 0.122$ kJ mol^{-1} for $\theta_{in} = 60°$ (black line in Fig. 4a). For $\theta_{in} = 75°$, 90°, 105° and 120°, the obtained free-energy barriers are $\Delta G_{cw} = 0.404$ kJ mol^{-1}, 0.686 kJ mol^{-1}, 1.594 kJ mol^{-1} and 3.724 kJ mol^{-1}, respectively (Fig. 4a). These results indicate that the intrinsic contact angle of the surface, θ_{in}, has a profound effect on the stability of the Cassie state. Specifically, the free-energy barrier for the Cassie-to-Wenzel state transition, ΔG_{cw}, varies exponentially with $\cos\theta_{in}$: $\Delta G_{cw}^{\varphi=45°} = 0.682\exp(-3.384\cos\theta_{in}) + 0.0015$ (black line in Fig. 5).

Finally, we computed the free-energy barriers for systems with $\varphi = 60°$ for purposes of comparison. In this case, surfaces with intrinsic contact angles (θ_{in}) of 90°, 100° and 110° were used (Fig. 4b). The raining simulations indicated a free-energy barrier of $\Delta G_{cw} = 0.309$ kJ mol^{-1} for $\theta_{in} = 90°$. This barrier is appreciably lower than the free-energy barrier ($\Delta G_{cw} = 0.686$ kJ mol^{-1}) obtained for $\varphi = 45°$ when $\theta_{in} = 90°$, indicating that the trapezoid base angle can strongly affect the stability of the Cassie state. Further simulations showed that the free-energy barriers for the Cassie-to-Wenzel state transition are $\Delta G_{cw} = 0.584$ kJ mol^{-1} and 1.398 kJ mol^{-1} for $\theta_{in} = 100°$ and $\theta_{in} = 110°$, respectively, when $\varphi = 60°$, both being much higher than that for $\theta_{in} = 90°$ when $\varphi = 60°$, thereby further proving the strong effect of the intrinsic contact angle on the stability of

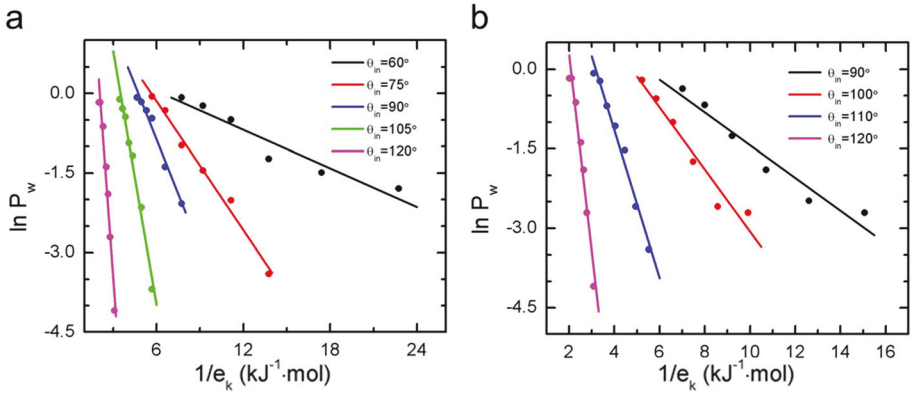

Fig. 4 Straight-line fits to ln P_w (probability of the Wenzel state) *versus* the reciprocal of the kinetic energy of the centre of mass of a water droplet with 24 256 water molecules. Trapezoid base angles of φ = 45° (a) and φ = 60° (b) were used in the raining simulations. In addition, several intrinsic contact angles were selected for the simulated solid surfaces.

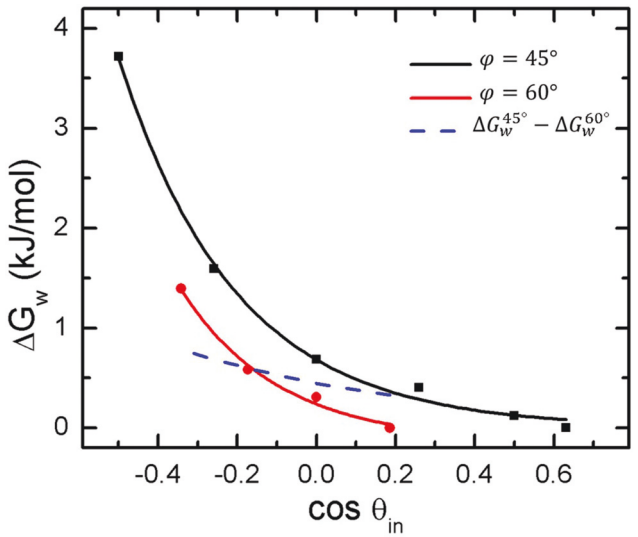

Fig. 5 Variation of the calculated free-energy barrier for the Cassie-to-Wenzel state transition *versus* the cosine of the intrinsic contact angle as obtained from MD simulations for φ = 45° (black squares) and φ = 60° (red circles). The solid black and red lines represent exponential fits to cos θ_{in}. The difference between the free-energy barriers for φ = 45° and φ = 60° is plotted as the dashed blue line.

the Cassie state. From the exponential curve fitted to the results for ΔG_{cw} *versus* cos θ_{in} when φ = 60°, one can deduce the following function: $\Delta G_{cw}^{\varphi=60^\circ} = 0.386\exp(-4.040\cos\theta_{in}) + 0.148$ (red line in Fig. 5). The difference between the free-energy barriers for φ = 60° and φ = 45° ($\Delta G_{cw}^{\varphi=45^\circ} - \Delta G_{cw}^{\varphi=60^\circ}$) was also calculated as a function of cos θ_{in} (dashed blue line in Fig. 5). Interestingly, this difference increases as θ_{in} increases, indicating that the base angle (φ) plays a more important role in determining the stability of the Cassie state as the intrinsic contact angle increases.

Lastly, we performed another series of MD simulations to study the influence of the length of each trapezoid unit on the wetting transition. Here the trapezoid base angle is fixed at φ = 90°. Two conditions are considered: one with fixed W = 24 Å (ESI Fig. S9a–c†) and another with fixed $S - W$ = 16 Å (ESI Fig. S9d–f†). The initial location for the water cube is on top of the pillars. Snapshots of the equilibrated droplet at t = 2.0 ns for these systems are shown in Fig. S9.† When W is fixed, the critical intrinsic contact angle for the Cassie-to-Wenzel state transition shows a large variation with respect to the $S - W$, with θ_{in}^{cw} increasing as $S - W$ increases (ESI Fig. S9a–c†). However, when the $S - W$ is fixed, the critical intrinsic contact angle for the Cassie-to-Wenzel state transition (θ_{in}^{cw}) is estimated about the same, which is equal to 106.1° ± 1.3°, regardless of the value of W (ESI Fig. S9d–f†).

3. Conclusions

MD simulations of a water nanodroplet on a nanostructured surface covered with a periodic array of trapezoids were performed to examine the effects of the base angle of the trapezoids and the intrinsic contact angle of the surface on the wetting state of the droplet. For a given trapezoid base angle, there exists a critical intrinsic contact angle below which water droplets on the surface can exist only in the Wenzel state. A strong base-angle dependence of this critical intrinsic contact angle is observed. Moreover, MD simulations with the water droplet being initially in the Wenzel state show that there is another critical intrinsic contact angle, above which water droplets on the surface can be stable only in the Cassie state. In contrast to the first critical intrinsic contact angle, this second critical intrinsic contact angle shows little dependence on the trapezoid base angle.

When the intrinsic contact angle of the surface is between the two critical intrinsic contact angles for a given base angle, water droplets on the surface exist in a bistable Wenzel–Cassie regime. The free-energy barrier for the transition from the Cassie to the Wenzel state, as computed based on raining simulations, exhibits a strong dependence on both the base angle of the trapezoids and the intrinsic contact angle of the surface. Specifically, the free-energy barrier for the Cassie-to-Wenzel state transition varies exponentially with the cosine of the intrinsic

contact angle of the surface for a given base angle. The quantitative results obtained from the simulations indicate that the Cassie state can be achieved on such a nanostructured hydrophilic substrate by suitably controlling the trapezoid base angle. Hence, our findings will benefit the future design of superhydrophobic surfaces fabricated with hydrophilic materials for practical applications in nanofluidics and surface coatings.

Conflicts of interest

There are no conflicts to declare.

Acknowledgements

This study is supported by the US National Science Foundation (CHE-1665324). The computational work was performed at the University of Nebraska Holland Computing Center.

References

1 R. Blossey, *Nat. Mater.*, 2003, **2**, 301–306.
2 P. Tabeling, *Lab Chip*, 2009, **9**, 2428–2436.
3 L. Ionov, N. Houbenov, A. Sidorenko, M. Stamm and S. Minko, *Adv. Funct. Mater.*, 2006, **16**, 1153–1160.
4 A. R. Betz, J. Jenkins, C. J. Kim and D. Attinger, *Int. J. Heat Mass Transfer*, 2013, **57**, 733–741.
5 Z. X. Xue, S. T. Wang, L. Lin, L. Chen, M. J. Liu, L. Feng and L. Jiang, *Adv. Mater.*, 2011, **23**, 4270–4273.
6 Y. X. Zhuang, O. Hansen, T. Knieling, C. Wang, P. Rombach, W. Lang, W. Benecke, M. Kehlenbeck and J. Koblitz, *J. Microelectromech. Syst.*, 2007, **16**, 1451–1460.
7 T. Nishino, M. Meguro, K. Nakamae, M. Matsushita and Y. Ueda, *Langmuir*, 1999, **15**, 4321–4323.
8 C. Q. Zhu, Y. R. Gao, H. Li, S. Meng, L. Li, J. S. Francisco and X. C. Zeng, *Proc. Natl. Acad. Sci. U. S. A.*, 2016, **113**, 12946–12951.
9 Y. F. Huang, Y. Hu, C. Q. Zhu, F. Zhang, H. Li, X. H. Lu and S. Meng, *Adv. Mater. Interfaces*, 2016, **3**, 1500727.
10 Y. S. Li, D. Quere, C. J. Lv and Q. S. Zheng, *Proc. Natl. Acad. Sci. U. S. A.*, 2017, **114**, 3387–3392.
11 R. N. Wenzel, *Ind. Eng. Chem.*, 1936, **28**, 988–994.
12 A. B. D. Cassie and S. Baxter, *Trans. Faraday Soc.*, 1944, **40**, 0546–0550.
13 T. Y. Liu and C. J. Kim, *Science*, 2014, **346**, 1096–1100.
14 A. Tuteja, W. Choi, M. L. Ma, J. M. Mabry, S. A. Mazzella, G. C. Rutledge, G. H. McKinley and R. E. Cohen, *Science*, 2007, **318**, 1618–1622.
15 C. Josserand and S. T. Thoroddsen, *Annu. Rev. Fluid Mech.*, 2016, **48**, 365–391.
16 T. Koishi, K. Yasuoka, S. Fujikawa, T. Ebisuzaki and X. C. Zeng, *Proc. Natl. Acad. Sci. U. S. A.*, 2009, **106**, 8435–8440.
17 J. Choi, W. Cho, Y. S. Jung, H. S. Kang and H. T. Kim, *ACS Nano*, 2017, **11**, 1320–1327.
18 A. Nakajima, A. Fujishima, K. Hashimoto and T. Watanabe, *Adv. Mater.*, 1999, **11**, 1365–1368.
19 K. Tadanaga, J. Morinaga, A. Matsuda and T. Minami, *Chem. Mater.*, 2000, **12**, 590–592.
20 L. Feng, S. H. Li, Y. S. Li, H. J. Li, L. J. Zhang, J. Zhai, Y. L. Song, B. Q. Liu, L. Jiang and D. B. Zhu, *Adv. Mater.*, 2002, **14**, 1857–1860.
21 L. Feng, Y. L. Song, J. Zhai, B. Q. Liu, J. Xu, L. Jiang and D. B. Zhu, *Angew. Chem., Int. Ed.*, 2003, **42**, 800–802.
22 H. Y. Erbil, A. L. Demirel, Y. Avci and O. Mert, *Science*, 2003, **299**, 1377–1380.
23 A. Lafuma and D. Quere, *Nat. Mater.*, 2003, **2**, 457–460.
24 Y. T. Cheng and D. E. Rodak, *Appl. Phys. Lett.*, 2005, **86**, 144101.
25 E. Hosono, S. Fujihara, I. Honma and H. S. Zhou, *J. Am. Chem. Soc.*, 2005, **127**, 13458–13459.
26 Z. G. Guo, F. Zhou, J. C. Hao and W. M. Liu, *J. Am. Chem. Soc.*, 2005, **127**, 15670–15671.
27 C. Yang, U. Tartaglino and B. N. J. Persson, *Phys. Rev. Lett.*, 2006, **97**, 116103.
28 T. Koishi, K. Yasuoka, S. Fujikawa and X. C. Zeng, *ACS Nano*, 2011, **5**, 6834–6842.
29 C. Frankiewicz and D. Attinger, *Nanoscale*, 2016, **8**, 3982–3990.
30 C. Neinhuis and W. Barthlott, *Ann. Bot.*, 1997, **79**, 667–677.
31 X. F. Gao and L. Jiang, *Nature*, 2004, **432**, 36–36.
32 J. Genzer and A. Marmur, *MRS Bull.*, 2008, **33**, 742–746.
33 A. Marmur, *Langmuir*, 2003, **19**, 8343–8348.
34 M. Nosonovsky, *Langmuir*, 2007, **23**, 9919–9920.
35 M. Nosonovsky, *Langmuir*, 2007, **23**, 3157–3161.
36 J. Bico, U. Thiele and D. Quere, *Colloids Surf., A*, 2002, **206**, 41–46.
37 A. Otten and S. Herminghaus, *Langmuir*, 2004, **20**, 2405–2408.
38 U. Mock, R. Forster, W. Menz and J. Ruhe, *J. Phys.: Condens. Matter*, 2005, **17**, S639–S648.
39 S. Herminghaus, *Europhys. Lett.*, 2000, **52**, 165–170.
40 M. F. Zhu, W. W. Zuo, H. Yu, W. Yang and Y. M. Chen, *J. Mater. Sci.*, 2006, **41**, 3793–3797.
41 H. Bellanger, T. Darmanin, E. T. de Givenchy and F. Guittard, *Chem. Rev.*, 2014, **114**, 2694–2716.
42 J. L. Liu, X. Q. Feng, G. F. Wang and S. W. Yu, *J. Phys.: Condens. Matter*, 2007, **19**, 356002.
43 V. Molinero and E. B. Moore, *J. Phys. Chem. B*, 2009, **113**, 4008–4016.
44 A. Reinhardt and J. P. K. Doye, *J. Chem. Phys.*, 2012, **136**, 054501.
45 E. B. Moore, J. T. Allen and V. Molinero, *J. Phys. Chem. C*, 2012, **116**, 7507–7514.
46 E. B. Moore and V. Molineroa, *J. Chem. Phys.*, 2010, **132**, 244504.
47 E. B. Moore and V. Molinero, *Nature*, 2011, **479**, 506–U226.
48 A. Hudait and V. Molinero, *J. Am. Chem. Soc.*, 2014, **136**, 8081–8093.
49 S. Plimpton, *J. Comput. Phys.*, 1995, **117**, 1–19.
50 C. Q. Zhu, H. Li, Y. F. Huang, X. C. Zeng and S. Meng, *Phys. Rev. Lett.*, 2013, **110**, 126101.
51 W. Xiong, J. Z. Liu, Z. L. Zhang and Q. S. Zheng, *Acta Mech. Sin. Prc*, 2013, **29**, 543–549.